



HAL
open science

Rubidium distribution at atomic scale in high efficient Cu(In,Ga)Se₂ thin-film solar cells

Arantxa Vilalta-Clemente, Mohit Raghuwanshi, Sébastien Duguay, Celia Castro, Emmanuel Cadel, Philippe Pareige, Philip Jackson, Roland Wuerz, Dimitrios Hariskos, Wolfram Witte

► To cite this version:

Arantxa Vilalta-Clemente, Mohit Raghuwanshi, Sébastien Duguay, Celia Castro, Emmanuel Cadel, et al.. Rubidium distribution at atomic scale in high efficient Cu(In,Ga)Se₂ thin-film solar cells. Applied Physics Letters, 2018, 112 (10), pp.103105. 10.1063/1.5020805 . hal-01929133

HAL Id: hal-01929133

<https://hal.science/hal-01929133v1>

Submitted on 23 May 2024

HAL is a multi-disciplinary open access archive for the deposit and dissemination of scientific research documents, whether they are published or not. The documents may come from teaching and research institutions in France or abroad, or from public or private research centers.




L'archive ouverte pluridisciplinaire **HAL**, est destinée au dépôt et à la diffusion de documents scientifiques de niveau recherche, publiés ou non, émanant des établissements d'enseignement et de recherche français ou étrangers, des laboratoires publics ou privés.



Distributed under a Creative Commons Attribution 4.0 International License

RESEARCH ARTICLE | MARCH 09 2018

Rubidium distribution at atomic scale in high efficient Cu(In,Ga)Se₂ thin-film solar cells

Arantxa Vilalta-Clemente; Mohit Raghuwanshi ; Sébastien Duguay ; Celia Castro ; Emmanuel Cadel; Philippe Pareige; Philip Jackson; Roland Wuerz; Dimitrios Hariskos; Wolfram Witte

 Check for updates

Appl. Phys. Lett. 112, 103105 (2018)

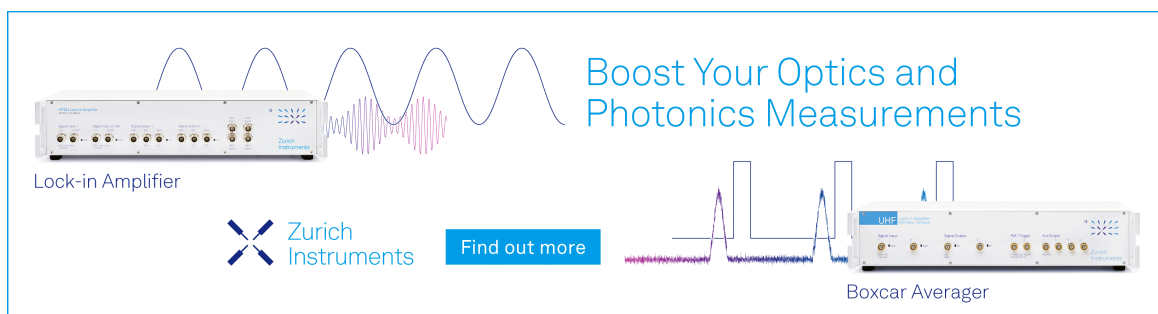
<https://doi.org/10.1063/1.5020805>



View Online




Export Citation



Boost Your Optics and Photonics Measurements

Lock-in Amplifier

 Zurich Instruments

[Find out more](#)

Boxcar Averager

Rubidium distribution at atomic scale in high efficient Cu(In,Ga)Se₂ thin-film solar cells

Arantxa Vilalta-Clemente,^{1,a)} Mohit Raghuwanshi,^{1,2,a)} Sébastien Duguay,¹ Celia Castro,^{1,b)} Emmanuel Cadet,¹ Philippe Pareige,¹ Philip Jackson,³ Roland Wuerz,³ Dimitrios Hariskos,³ and Wolfram Witte³

¹Groupe de Physique des Matériaux, Normandie Univ, UNIROUEN, INSARouen, CNRS 6634, 76000 Rouen, France

²RWTH Aachen, I. Physikalisches Institut IA, Sommerfeldstr. 14, 52074 Aachen, Germany

³Zentrum für Sonnenenergie- und Wasserstoff-Forschung Baden-Württemberg (ZSW), Meitnerstr. 1, 70563 Stuttgart, Germany

(Received 27 December 2017; accepted 20 February 2018; published online 9 March 2018)

The introduction of a rubidium fluoride post deposition treatment (RbF-PDT) for Cu(In,Ga)Se₂ (CIGS) absorber layers has led to a record efficiency up to 22.6% for thin-film solar cell technology. In the present work, high efficiency CIGS samples with RbF-PDT have been investigated by atom probe tomography (APT) to reveal the atomic distribution of all alkali elements present in CIGS layers and compared with non-treated samples. A Scanning Electron Microscopy Dual beam station (Focused Ion Beam–Gas Injection System) as well as Transmission Kikuchi diffraction is used for atom probe sample preparation and localization of the grain boundaries (GBs) in the area of interest. The analysis of the 3D atomic scale APT reconstructions of CIGS samples with RbF-PDT shows that inside grains, Rb is under the detection limit, but the Na concentration is enhanced as compared to the reference sample without Rb. At the GBs, a high concentration of Rb reaching 1.5 at. % was found, and Na and K (diffusing from the glass substrate) are also segregated at GBs but at lower concentrations as compared to Rb. The intentional introduction of Rb leads to significant changes in the chemical composition of CIGS matrix and at GBs, which might contribute to improve device efficiency. © 2018 Author(s). All article content, except where otherwise noted, is licensed under a Creative Commons Attribution (CC BY) license (<http://creativecommons.org/licenses/by/4.0/>).
<https://doi.org/10.1063/1.5020805>

Recent progress has been made to polycrystalline Cu(In,Ga)Se₂ (CIGS) thin film solar cell efficiency, pushing the record above 22% with heavy alkali metal post deposition treatment (PDT) of the CIGS absorber layer¹ and molybdenum-coated alkali-aluminosilicate glass substrate (Na and K).¹ These alkali elements are known to diffuse into the polycrystalline CIGS absorber through the Mo back contact during CIGS growth at elevated temperatures,^{2,3} enhancing photovoltaic properties of CIGS solar cells.⁴ It has been recently demonstrated, using atom probe tomography (APT), that Na accumulates at grain boundaries (GBs) of polycrystalline CIGS layers.⁵ A segregation level (or Gibbsian interfacial excess, Γ) of 2.2 atoms/nm² in average at the GB has been measured.⁶ Besides, a very small optimum amount of Na is necessary for better performances, whereas an overdose of its incorporation might result in degraded device performance.⁷ A Na amount of 60 ppm diffuses into the grain interiors.⁸ Concerning potassium, APT investigations revealed^{8–10} an increased concentration at GBs.

Having now in addition RbF-PDT in the process, an updated picture of the chemical composition of alkali metals at the GBs and inside the grains is needed. In this letter, we present a comparative atomic scale study of CIGS thin films with and without RbF-PDT, allowing the compositional distribution of the alkali metals within the grains and at GBs to

be obtained and quantified. APT results are also compared with density functional theory (DFT) modeling in the literature, and the effect of alkali segregation at GBs and on the overall GB chemistry is also discussed.

CIGS solar cells studied in this work were fabricated by a co-evaporation technique using a multistage process. After the synthesis of CIGS thin films, two series of samples were prepared: (i) with RbF-PDT similar to the procedure employed in Ref. 11 and (ii) with no-PDT. Completion of the solar cell was identical in both cases, and more details about different layers and their preparation can be found in the work of Jackson *et al.*¹

Samples in the shape of tips were prepared using a Scanning Electron Microscopy (SEM) dual beam station [Focused Ion Beam–Gas Injection System (FIB–GIS)–Zeiss Nvision40] for correlative APT/transmission Kikuchi diffraction (TKD). In order to analyze the CIGS absorber by APT, tips were extracted parallel to the Mo/Glass substrate increasing the probability of observing GBs by standard FIB-based lift out and annular milling protocols.¹² Low kV (2 kV) ion cleaning was performed at the end to minimize FIB-induced damages.

In order to ensure the analysis of a GB interface and to determine the misorientation angle between two grains, TKD measurements were performed directly on the tip after annular milling at an acceleration voltage of 20 kV and a SEM probe current of 1 nA. TKD maps were recorded using 2 × 2 binning with an exposure time of 43 ms and a step size of 50 nm. In order to localize the GB within the first 100–150 nm of the tip,

^{a)}A. Vilalta-Clemente and M. Raghuwanshi contributed equally to this work.

^{b)}celia.castro@univ-rouen.fr

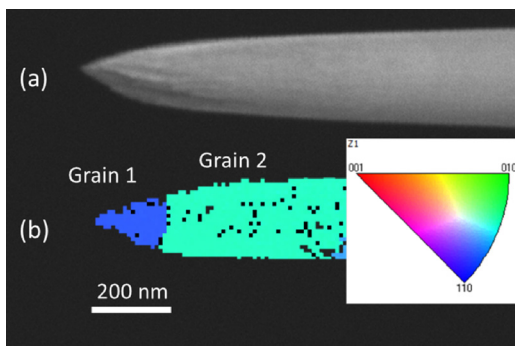


FIG. 1. Overview (a) SEM image of the CIGS atom probe tip (RbF-PDT sample) prepared by FIB milling from a region of the CIGS absorber close to the Mo back contact of a complete solar cell stack. (b) TKD inverse pole figure map plotted along the z-axis (legend on the right) showing the presence of a high-angle GB.

the tip apex was milled by imaging the sample with a 2 kV-Ga beam until the GB interface reaches the desired location.

APT was performed using a laser assisted wide angle tomographic atom probe (LaWaTAP) with a flight length of

10 cm.¹³ Atom probe specimens were analyzed at a temperature of 60 K and field evaporated using femtosecond laser pulses ($\lambda = 515$ nm) with a repetition rate of 100 kHz and a laser energy of 10 nJ. The 3D reconstructions and data mining were performed using home built GPM3Dsoft software.

After atom probe tip sample preparation as depicted in Fig. 1(a), TKD has been used to determine the precise location and misorientation of the GB. The Inverse Pole Figure (in the Z direction, i.e., the tip axis) map (IPFZ) shows the existence of two grains (Grain 1 and Grain 2) with different crystallographic orientations by appearing in different colors [refer to the color legend in Fig. 1(b)]. The misorientation between both grains in Fig. 1(b) indicates the presence of a high-angle GB. Note that the misorientation is 51° here.

Figure 2(a) (multimedia view) depicts a 3D distribution map resulting from the APT analysis of a RbF-PDT sample that contains a GB (see video associated). Only the distribution of alkali metal atoms is shown for clarity ($^{85}\text{Rb}^+$: orange, $^{39}\text{K}^+$: purple, and $^{23}\text{Na}^+$: black). This atomic map clearly reveals the presence of the GB where a strong planar segregation of Rb

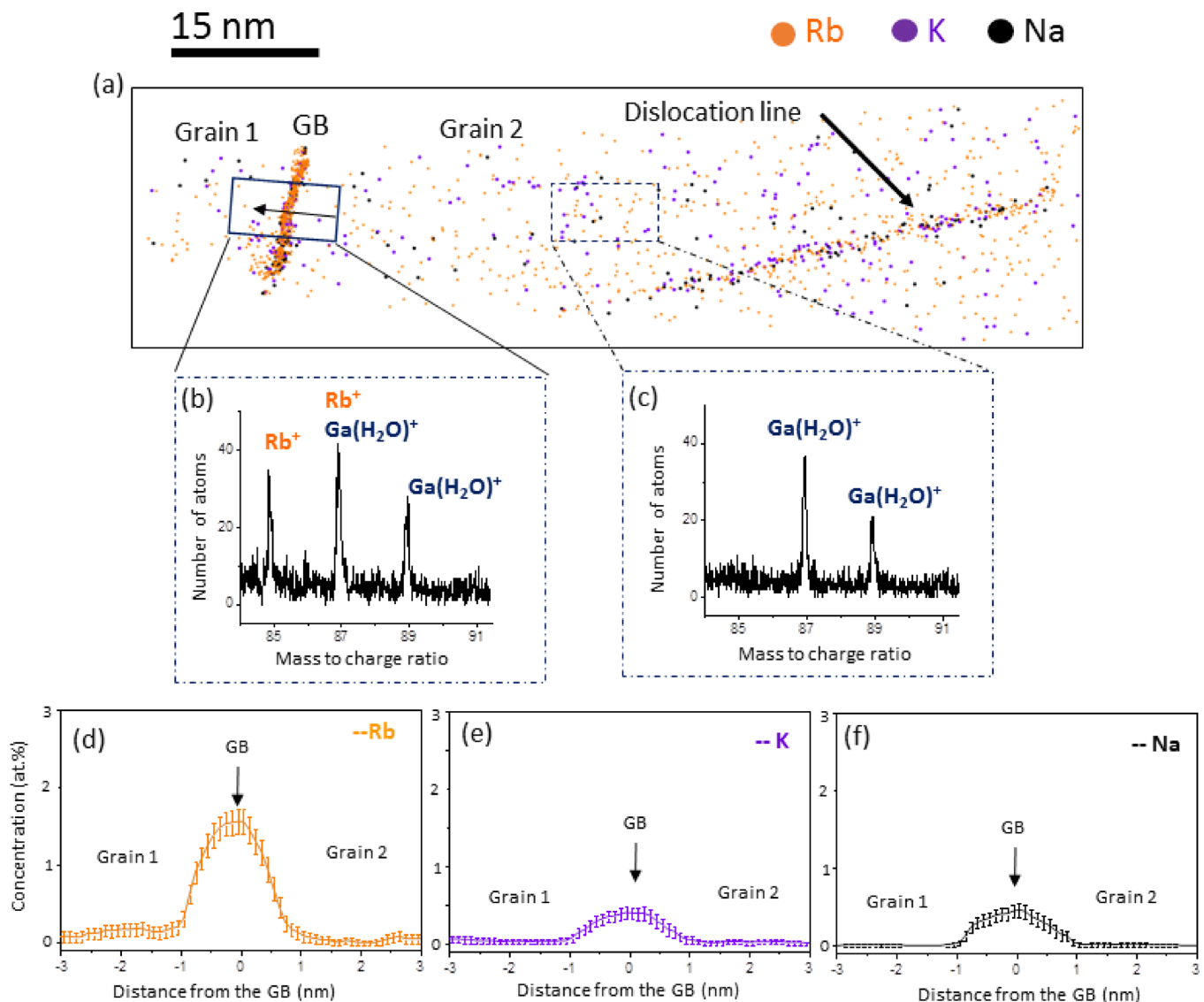


FIG. 2. (a) Reconstructed atom probe tip depicted in Fig. 1 after analysis (RbF-PDT sample). Only $^{85}\text{Rb}^+$, $^{39}\text{K}^+$, and $^{23}\text{Na}^+$ are shown for better visualization of the GB. Each dot represents an individual atom and the different colors represent the respective chemical species. The mass spectrum from 84 to 91 a.m.u depicts the presence of Rb in two regions: (b) at the GB and (c) within the grain. (d)–(f) Line across the GB from the parallelepiped in (a) showing the alkali metals Rb, K, and Na, respectively. Multimedia view: <https://doi.org/10.1063/1.5020805.1>

TABLE I. Power conversion efficiencies, mean Gibbsian interfacial excess (Γ) values at GBs, and chemical composition inside the grains for the alkali metals (RbF-PDT and no-PDT samples). APT tips of the RbF-PDT sample were prepared from a complete solar cell stack and for the no-PDT sample from a glass/Mo/CIGS/CdS stack, i.e., all samples were exposed to an ammonia-containing CdS chemical bath deposition. ARC: anti-reflective coating.

Sample	Efficiency (%)	At GBs- Γ (at/nm ²)			Chemical composition inside the grains (ppm)		
		Rb	Na	K	Rb	Na	K
RbF-PDT	21.1 (w/ARC)	1.6 ± 0.4	0.4 ± 0.1	0.4 ± 0.1	u.d.l. ^a	39 ± 4	u.d.l
No-PDT	19.5 (w/o ARC)		1.2 ± 0.4	0.5 ± 0.2		15 ± 5	u.d.l

^au.d.l. under the detection limit. K below 20 ppm, Na below 5 ppm, and Rb below 10 ppm.

atoms is highlighted. Figure 2(a) (multimedia view) shows the location where sampling boxes were used to extract the concentration profiles. Figures 2(b) and 2(c) (multimedia view) allow direct comparison of isotope distribution at the GB and within the “Grain 2,” respectively. Mass spectra are restricted to the 84–91 atomic mass units (a.m.u.) area of interest. Indeed, Rb exists with two isotopes (85 a.m.u. and 87 a.m.u.) and usually appears to these both mass to charge ratios (85 and 87) being mostly ionized as singly charged. It must be noted that the latter peak at 87 is convoluted with the complex Ga(H₂O)⁺ peak [see Fig. 2(b) (multimedia view)]. A standard correction based on the isotopic ratio distribution has been applied on the composition profile and quantification of compositions. The peak at 23 a.m.u. was assigned to Na and that at 39 a.m.u. and 41 a.m.u. was attributed to K (mass spectrum not shown). However, it must be noted that the peak at 39 a.m.u. and 41 a.m.u. might also be a consequence of the detection of Se²⁺ or the molecular ion NaO. To resolve this issue, an isotopic peak deconvolution was done to determine the amount of K. Due to this overlap, the detection limit for K is only about 20 ppm. Oxygen segregation was not found at the GBs.

In order to calculate the concentration profile of elements across the GB, a sampling volume of 10 × 10 × 25 nm³ was moved in steps of 0.1 nm in a direction perpendicular to the GB interface. The resulting concentration profile of alkali elements is displayed in Figs. 2(d)–2(f) (multimedia view). The maximum Rb content is about 1.5 at. %, while Na and K contents are both of the order of 0.4 at. %. In addition, as seen in Fig. 2 (multimedia view), a linear segregation of alkali elements was also observed inside Grain 2. This feature typically refers to the presence of a dislocation line in the analyzed volume, and the calculated Rb concentration is 0.5 at. % and for lighter alkali elements (Na and K) are 0.2 at. %. In the image, the artificial presence, Fig. 2(a) (multimedia view), of alkali atoms inside the grains is attributed to the background noise signal in these mass to charge windows as shown in Figs. 2(b) and 2(c) (multimedia view). Two separate 3D sampling volumes containing an equal number of atoms, one containing a GB [Fig. 2(b) (multimedia view)] and the other one inside the matrix [Fig. 2(c) (multimedia view)], clearly show detection of Rb and no detection of Rb above the background noise, respectively. As far as the grain interior is concerned, the Rb and K concentrations are under the detection limit (u.d.l.: K below 20 ppm and Rb below 10 ppm).

The Gibbsian interfacial excess Γ_i of an alkali i is calculated for several GBs. In total, seven GBs have been analyzed for RbF-PDT samples and three GBs for no-PDT samples. The excess is determined from a diagram along the analyzed volume, which presents a plot of the cumulative number of

alkali atoms with respect to the cumulative number of total atoms. An increase in the slope marks the segregation. Furthermore, the excess is normalized to the interface area.¹⁴

Table I highlights differences between the Gibbsian interfacial excesses of alkali elements at the GBs for RbF-PDT and no-PDT samples: (i) for the RbF-PDT, the amount of Na and K is similar (0.4 ± 0.1 at/nm²), whilst for the no-PDT, the Na amount (1.2 ± 0.4 at/nm²) is higher than the amount of K (0.5 ± 0.2 at/nm²). This finding clearly indicates the replacement of the lighter alkali element (Na) by heavier (Rb) at GB when a PDT is performed.

Due to the atomic convolution at peak 39 a.m.u., it is not very conclusive whether K is driven out of the GB or not, but overall, the resulting general observation is that the heavier Rb alkali element, which is intentionally introduced during the PDT process into the as-grown CIGS absorber, tends to push out the Na already present in the GBs. This result is supported by secondary ion mass spectrometry experiments^{1,15} and by recent density functional theory (DFT) modeling¹⁶ where heavier alkali elements drive out Na from the thin films. Our results show that these lighter alkali elements normally reside at the GBs, but the introduction of a heavier alkali element (Rb in this case) drives out and replaces a part of the lighter alkali elements at the GBs. Concerning Na, a higher concentration was found inside the grain (~40 ppm) for the RbF-PDT CIGS, as compared to the no-PDT (~15 ppm) sample. One of the reasons for this phenomenon could be the higher ionic radius of Rb as compared to K and Na which might be more energetically favorable to segregate at GBs, following observations from Sutton *et al.*¹⁷

Figure 3 shows the overall GB chemistry considering all elements present in the CIGS thin film. A Cu depletion and

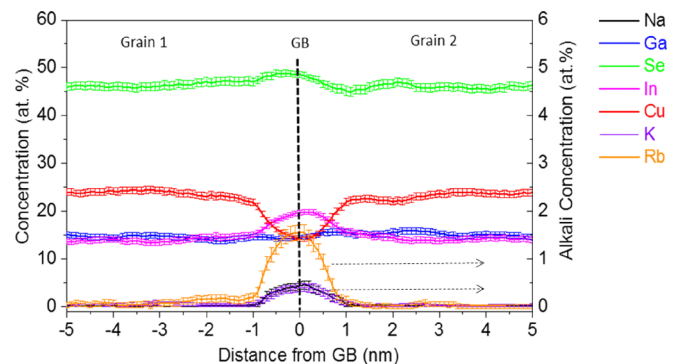


FIG. 3. Composition profile of CIGS matrix elements (left y-axis) and alkali elements (right y-axis) in the vicinity of the GB in Fig. 2 (multimedia view) (sample with RbF-PDT). A very strong copper depletion is measured at the GB.

an In enrichment are detected at the GB, and no significant variation in Ga and Se concentrations are observed in comparison to their matrix concentrations. The variation of the Cu concentration (ΔCu) is calculated by subtracting the Cu concentration at the GB (14.1 at. %) from the Cu concentration inside the grain (24.3 at. %). These concentration variations at GB have already been observed in previous studies.^{6,18} However, it must be noted here that the Cu depletion in the current case is much more pronounced than it has ever been recorded before. The Cu depletion in the present result reaches about $\Delta\text{Cu} = 42\%$ which is higher than a maximum of 30% depletion recorded in the literature.¹⁸ A higher Rb concentration at the GB also might indicate its occupation of some Cu sites at the GB.

Our previous studies¹⁸ have shown that changes in GB chemistry of matrix elements in CIGS have a significant influence on its performance and efficiency. Cu depletion at the GBs was directly linked to the improved device performance, while Cu enrichment at GBs generates more carrier recombination at GBs. Thus, the results here also indicate that the RbF-PDT may play a major role in improving the hole-barrier characteristics of GBs in CIGS.¹⁹

PDT with heavy alkali elements like Rb on CIGS thin films produces record efficiency cells. The improvement in the device performance due to PDT is assigned to a local atomic redistribution of matrix and alkali elements in the CIGS absorber layer. Here, owing to the APT, we show that the heavier alkali element (Rb) segregates at GBs and modifies the usual amount of lighter alkali elements (K and Na) and Cu content in these GB interfaces. This Rb segregation and coverage makes the GBs Cu deficient inducing a better hole barrier property and possibly improves the minority carrier collection at GBs and the overall cell performance.

Malitckaya *et al.*¹⁶ calculated the migration barriers for the alkali metals in CuInSe_2 in order to understand the atomic migration inside the grains during the PDT. The migration energy barriers show that the interstitial diffusion mechanism may be relevant only for Na and K, whereas the Rb atoms can diffuse by the help of the Cu vacancies. The competition between these two mechanisms strongly depends on the concentration of Cu vacancies. Based on their simulations, the heavier Rb atom dominates at the GB and no Rb atoms are displaced inside the grain. Their findings are supported by our experimental APT results for the samples with RbF-PDT. Recently, nano X-ray fluorescence (XRF) investigations of a CIGS absorber deposited on a Mo-coated ferritic stainless steel foil demonstrated that Rb diffuses along the GBs.²⁰

In this letter, we conducted APT measurements to investigate the alkali metal distribution in high efficiency

polycrystalline CIGS thin-film solar cells fabricated with similar co-evaporation processes but different PDT processes: (i) with RbF-PDT and (ii) the reference, no-PDT. In conclusion, we showed Rb segregation at the GBs by APT. For the lighter alkali, the Na concentration at the GBs is higher for the non-treated sample compared to the RbF treated sample and the K concentration at GBs is similar for both samples. This finding clearly indicates the replacement of the lighter alkali element (Na) by the heavier Rb. Our results also show a strong depletion of the Cu content at a GB, most likely induced by the diffusion of Rb into the GB.

This project has received funding from the European Union's Horizon 2020 research and innovations program under Grant Agreement No. 641004 (SharC25).

¹P. Jackson, R. Wuerz, D. Hariskos, E. Lotter, W. Witte, and M. Powalla, *Phys. Status Solidi-RRL* **10**, 583 (2016).

²R. Wuerz, A. Eicke, F. Kessler, S. Paetel, S. Efimenko, and C. Schlegel, *Sol. Energy Mater. Sol. Cells* **100**, 132 (2012).

³S. Ishizuka, A. Yamada, P. J. Fons, H. Shibata, and S. Niki, *ACS-Appl. Mater. Interfaces* **6**, 14123 (2014).

⁴J. Hedström, H. Ohlsén, M. Bodegård, A. Kylner, L. Stolt, D. Hariskos, M. Ruckh, and H.-W. Schock, in *23rd IEEE Photovoltaic Specialists Conference* (1993), p. 364.

⁵E. Cadel, N. Barreau, J. Kessler, and P. Pareige, *Acta Mater.* **58**, 2634 (2010).

⁶M. Raghuvanshi, E. Cadel, S. Duguay, L. Arzel, N. Barreau, and P. Pareige, *Prog. Photovolt.: Res. Appl.* **25**, 367 (2017).

⁷X. H. Tan, S. L. Ye, B. Fan, K. Tang, and X. Liu, *Appl. Opt.* **49**, 3071 (2010).

⁸O. Cojocaru-Mirédin, T. Schwarz, P. Choi, M. Herbig, R. Wuerz, and D. Raabe, *J. Vis. Exp.* **74**, e50376 (2013).

⁹A. Stokes, M. Al-Jassim, D. Diercks, and B. Gorman, in *IEEE 42nd Photovoltaic Specialist Conference, PVSC* (2015), p. 1.

¹⁰A. Stokes, M. Al-Jassim, and B. Gorman, *Microsc. Microanal.* **22**, 644 (2016).

¹¹A. Chirilă, P. Reinhard, F. Pianezzi, P. Bloesch, A. R. Uhl, C. Fella, L. Kranz, D. Keller, C. Gretener, H. Hagendorfer *et al.*, *Nat. Mater.* **12**, 1107 (2013).

¹²M. K. Miller, K. F. Russell, and G. B. Thompson, *Ultramicroscopy* **102**, 287 (2005).

¹³B. Decanilhout, F. Vurpillot, B. Gault, G. Da Costa, M. Bouet, A. Bostel, D. Blavette, A. Hideur, G. Martel, and M. Brunel, *Surf. Interface Anal.* **39**, 278 (2007).

¹⁴O. C. Hellman and D. N. Seidman, *Mater. Sci. Eng. A* **327**, 24 (2002).

¹⁵P. Reinhard, B. Bissig, F. Pianezzi, E. Avancini, H. Hagendorfer, D. Keller, P. Fuchs, M. Döbeli, C. Vigo, P. Crivelli *et al.*, *Chem. Mater.* **27**, 5755 (2015).

¹⁶M. Malitckaya, H.-P. Komsa, V. Havu, and M. J. Puska, *J. Phys. Chem. C* **121**, 15516 (2017).

¹⁷A. P. Sutton and V. Vitek, *Acta Metall.* **30**, 2011 (1982).

¹⁸M. Raghuvanshi, E. Cadel, P. Pareige, S. Duguay, F. Couzinie-Devy, L. Arzel, and N. Barreau, *Appl. Phys. Lett.* **105**, 013902 (2014).

¹⁹C. Persson and A. Zunger, *Phys. Rev. Lett.* **91**, 266401 (2003).

²⁰P. Schöppe, S. Schönherr, R. Wuerz, W. Wisniewski, G. Martínez-Criado, M. Ritter, K. Ritter, C. Ronning, and C. S. Schnorr, *Nano Energy* **42**, 307 (2017).